TEMPORAL DILATION OF ANIMAL CARDIAC RECORDINGS REGISTERED TO HUMAN TORSO GEOMETRIES

by

Karli K. Gillette

A thesis submitted to the faculty of
The University of Utah
in partial fulfillment of the requirements for the degree of

Master of Science

Department of Bioengineering

The University of Utah

December 2016

The University of Utah Graduate School

STATEMENT OF THESIS APPROVAL

The thesis of Karli K. Gillette
has been approved by the following supervisory committee members:

Robert S. Macleod	, Chair	09/01/2016 Date Approved
Frank Sachse	, Member	09/01/2016 Date Approved
Ravi Ranjan	, Member	09/01/2016 Date Approved
Jeff Wilkinson	, Member	09/21/2016 Date Approved

and by Patrick A. Tresco, Chair/Dean of
the Department/College/School of Bioengineering
and by David B. Kieda, Dean of The Graduate School.

ABSTRACT

This study introduces a pipeline for the temporal dilation of canine cardiac signals following registration to human torsos. Performing registration of data attained from canine electrophysiology studies to human torso geometries allows for a larger database for the investigation of human-like arrhythmias that cannot be readily obtained otherwise. However, during registration, the canine cardiac signals must be adjusted to correct spatially dependent aspects of propagation, such as conduction velocity (CV), that are influenced by increased heart size. We refer to this correction process as "temporal dilation" as it includes resampling of the cardiac signals.

We acquired 10 canine cardiac recordings from electrodes built into socks that covered the epicardial surface of the ventricles. The sock geometries were registered to two human torsos. From this spatial transform, we calculated both global and local scaling factors needed to adjust the time signals. Signals were then dilated with both scaling types using linear and nonlinear techniques. The linear method homogeneously dilated the entire signal and the nonlinear technique dilated segments of the signals outside the QRS and T wave. Dilated cardiac signals were validated by comparison of calculated values of CV, total activation time (TAT), and activation recovery interval (ARI). Activation maps also served as a means of qualitative comparison.

The observed ECG metrics of canine cardiac signals after temporal dilation using global scaling closely resembled those from human recordings in terms of CV, ARI, and TAT. Temporally dilated signals using local scaling, in contrast, caused the observed ECG metrics to no longer remain within a physiologically relevant range. A realistic activation pattern was maintained after temporal dilation using global scaling.

Though temporal dilation using locally calculated scaling factors did not result in physiologically relevant cardiac signals to humans, homogenous temporal dilation could be used to correct the spatially dependent aspects of propagation after geometric registration of canine hearts to human torso geometries. Homogenous temporal dilation, therefore, is a technique that can be used to generate human-like cardiac signals useful for validation of devices used to diagnose, monitor, or intervene in cases of cardiac arrhythmias.

For my family and friends.

CONTENTS

LIST OF TABLES

LIST OF FIGURES

ACKNOWLEDGMENTS

First and foremost, I would like to acknowledge Medtronic Inc. for both funding and providing the motivation behind this research. The collaboration with Medtronic Inc. would not be possible without Jeff Wilkinson, who not only helped cultivate a productive and successful relationship, but ensured the research remained clinically relevant.

This research would also not be possible without the guidance and continuous support from my graduate advisor, Dr. Rob MacLeod. He has indisputably played a significant role throughout this research by providing constructive criticism and feedback. Additionally, he has given me opportunities throughout both my undergraduate and graduate career that I couldn't be more grateful for.

I would also like to thank Jess Tate at the SCI Institute for contributing a substantial amount of work and insight on this project.

Lastly, I must thank my family and friends. While my family taught me the value of an education at an early age and always encouraged me to pursue my academic goals, my friends, both here in Salt Lake City and abroad, have taught me what it means to have the strength to accomplish those goals.

CHAPTER 1

INTRODUCTION

1.1 Cardiac Anatomy and Function

The heart, the primary mechanical driver of the cardiovascular system, is responsible for pumping blood throughout the human body. The human heart has four chambers: two ventricles and two atria. The ventricles provide the main pumping acton and the atria collect the blood from the body [1]. Pumping of the heart stems from the ability of the myocardium, the general name for tissue within the heart, to receive and propagate bioelectric signals, which then determine mechanical contraction. The propagation of electrical waves through the myocardium signals the tissue to contract, which, when functioning properly, causes a coordinated contraction of the ventricles that pumps blood.

In a healthy heart, the activation of the myocardium is initiated by a group of self-excitatory cells within the sinoatrial node [2]. Each such cell generates an action potential that is characterized by the rapid depolarization of the transmembrane potential. This rapid depolarization causes closely connected myocardial cells to also depolarize, which creates what is termed a wave of depolarization [2]. The wave of depolarization spreads throughout the heart at a rate dictated by the conduction velocity (CV) of the tissue. The total time for all tissue in the heart to become activated is called total activation time (TAT), and the visualization of activation in the heart is called an activation map. The heart stays activated for a period of 200 to 300 ms and thus maintains contraction for a similar period [3]. Even after the subsequent electrical recovery or repolarization of the cells, they are not capable of reinitiating an action potential again for a period that is referred to as the refractory time. The duration that a cell remains depolarized with a raised transmembrane potential is termed the action potential duration. Its macroscopic (tissue scale) equivalent value is the activation recovery interval (ARI), and this value corresponds to the extracellular measurement of what is known as an electrogram (EG) from a region of myocardium.

1.2 Cardiac Disease States

Many disease states influence electrical propagation of activation in the heart and thus result in changes to CV, ARI, TAT, or activation maps. Myocardial ischemia is one such disease state, resulting from a lack of blood flow within the myocardial tissue of the heart that can cause the development of abnormal electrical activity at the cellular and tissue levels [4]. Prolonged ischemia can lead to permanent alteration of ionic currents that allow for action potential conduction or tissue necrosis, directly lowering or inhibiting cardiac propagation [5]. Such changes in conduction can lead to dangerous cardiac conditions, such as ventricular tachycardia (VT), an abnormal increase in heart rate, and even fibrillation (VF), the chaotic and ultimately fatal electrical and mechanical failure of the heart [1, 6].

Frequently, such conditions are monitored and diagnosed using technology such as the 12-lead electrocardiogram (ECG), which was originally utilized in the clinical detection of arrhythmias [7]. The ECG provides electrical recordings of cardiac electrical activity from the torso surface. After diagnosis of life threatening arrhythmias or substantial heart failure, intervention is often necessary in the form of implantable cardioverter defibrillators (ICDs). These devices consist of a implanted device with electrodes attached near the heart that record and store EGs to monitor cardiac electrical activity for arrhythmia and apply defibrillation shocks when necessary [8].

1.3 ECG Forward and Inverse Problems

Numerical and computer simulation of cardiac electrical activity plays an important role in modeling the various mechanisms of ventricular arrhythmias and thereby helps validate arrhythmia diagnostic and monitoring technologies such as the 12-lead ECG or ICD. The electrocardiographic forward and inverse problems are a generalized formalism for modeling the relationship between cardiac electrical activity and the associated body-surface potentials [9]. The forward problem uses surface-based or volume-based biophysical source descriptions of the heart, usually together with electrical potentials recorded from the heart to predict the body-surface ECG. The associated inverse problem, also known as ECG Imaging (ECGI), begins with measurements of body surface potentials and estimates from them the underlying cardiac electrical activity [10]. To perform computational simulation such as the ECG forward and inverse problems, geometrical models must be generated that are representative of both the torso and heart anatomies. Although models are inherently made from a single anatomy, registration can be used to geometrically align, and thus effectively combine, models from different hearts and geometries.

1.4 Motivation and Objectives

There is a major push to develop arrhythmia diagnostic and monitoring technologies that are relatively noninvasive such as ECGI, or possibly require semi-invasive measurements from recording locations accessible via venous catheters, such as the ICD. However, due to the invasive nature of obtaining EGs, training and validating such techniques or devices in humans is difficult, expensive, or unethical. Animal experiments provide an acceptable alternative to gather such data, and our research group has developed a pipeline to combine a database of past canine cardiac recordings of EGs with patient geometries.

The pipeline for combining canine heart data with human geometries requires geometric registration to map recording sites from the animal hearts to equivalent locations on the humans. However, during geometrical registration, electrode spacings change, creating artifacts in propagation behavior that lead to distortions in parameters such as CV, ARI, TAT, and activation maps. If the time signals recorded from the canine heart are unaltered, the resulting spatial organization of the spread of activation is distorted and CV values artificially increase. While it is known that CV within the ventricles is slightly higher in humans than in dogs, the calculated conduction values may increase past reasonable physiological values on the heart [11].

In this project, we propose a way of addressing the problem of altered cardiac propagation of canine cardiac signals due to registration by using temporal dilation in connection with the geometric size changes. Temporal dilation is the process of temporally expanding time series data by a scaling factor. In this case, such dilations allow for modification of activation times to ensure that the CV remains physiologically reasonable even when the canine signals are applied to humans. We will show that, by using temporal dilation, we can generate physiologically realistic cardiac signals that can help validate and support the development of new tools and methods for monitoring and intervening in cases of cardiac arrhythmias.

CHAPTER 2

TECHNICAL BACKGROUND

The key topic of temporal dilation is highlighted in the methods section (Chapter 3). Here we address the additional technical background topics of geometric model generation and the related steps of segmentation, meshing, registration, and interpretation of cardiac electrical recordings serving as the basis for temporal dilation.

2.1 Geometric Model Generation

The generation of geometric models used in cardiac simulation typically begins with medical images and ends with the generation of polygonal meshes [12] and thus depends heavily on the steps of both segmentation and meshing. Segmentation requires the assignment of constituent features related to organ or tissue types, such as the heart and torso, in a usually three-dimensional image to a set of nonintersecting regions [13]. Mesh quality, and subsequent simulation quality, is primarily dependent on the ability of the methods employed to extract elements from and properly detect boundary surfaces within the images [14].

From the segmentation, the next step is to place points or nodes at suitable intervals on all surfaces of interest, i.e., the boundaries between the different regions of the segmentation. The nodes are then connected into a surface mesh that is typically constructed of many (up to millions of) triangles or quadrilaterals. For some cases, it is also necessary to add more nodes to the volume of the mesh and connect these into tetrahedra or hexahedra [15, 16]. Once generated, each defined region in a mesh can be assigned differing properties, such as conductivity of electrical propagation during cardiac simulation.

Registration is the step of aligning geometrical elements that are initially in different coordinate systems, e.g., derived from different image data (e.g., MRI or CT) or perhaps even from different subjects. Though the choice of registration technique depends on the application, the simplest registration methods are typically linear, utilizing affine or rigid transformations, and require user-based selection of landmarks [17]. Landmarks are a defined set of coordinate locations at specific anatomical features within both images that define the constraints of the registration [18]. More advanced registration techniques

attempt to choose correspondence points automatically using the geometry of the objects being registered, for example, the iterative closest point (ICP) algorithm, which was the method used in this study to allow for the combination of torso and heart geometries [19]. All registration methods are, of course, approximations and optimal only in some least-squared-error sense. The user must always account for the consequences of the resulting errors, often through the use of additional approximation approaches such as interpolation of the data associated with the nodes or elements of the geometric model.

2.2 Interpretation of Cardiac Electrical Signals

Both EGs and ECGs provide a time signal of electrical potentials from the heart or body as sensed by pairs of electrodes in direct contact with the body. The acquisition of such signals can be in one of two modes, bipolar and unipolar, and the mode dictates the resulting interpretation of the signals. In bipolar measurements, the two electrodes are placed in proximity to each other (millimeters in the case of cardiac EGs), and the resulting time signal is sensitive only to local events; signal components common to both electrodes are subtracted and hence rejected. In unipolar measurements, there is an approximation of a neutral or remote reference electrode that is common to one or more measurements by means of single electrodes. These signals contain information from remote electrical events as well as local events arising near the sensing electrode. In both bipolar and unipolar signals, the waveform is dependent on the direction and timing of the wave of activation and deactivation in the tissue. Unique to the unipolar signals is the detection of a wave traveling toward the electrode or in the positive orientation of a lead, as a positive upstroke and vice versa. When the wave passes the location of the unipolar electrode, the signal deflects rapidly downwards, and this sharp feature is a robust indicator of the time of local depolarization of the action potential, also known as the activation time of the nearby tissue.

During normal spread of electrical activation in the heart, wave morphology recorded from EGs and ECGs is characterized by five primary deflections labeled as the P, Q, R, S, and T waves [20]. Depolarization of the atria and ventricles is denoted by the P wave and QRS complex, respectively [2]. The T wave primarily indicates the repolarization of the ventricles [2, 21]. EGs acquired either far from the base of the heart or from experimental setups without functioning atria lack a P-wave, as is the case in some experiments of this study (Fig. 2.1).

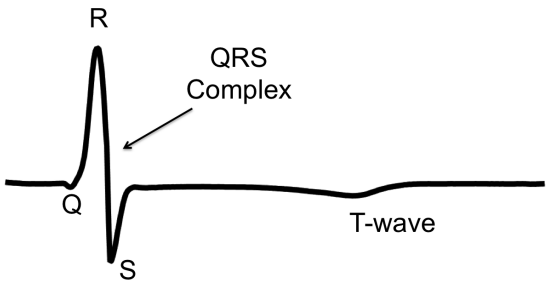

Figure 2.1: Representative recording of cardiac electrical activity labeled using the PQRST nomenclature.

The shape and amplitude of cardiac electrical signals depends strongly on the location of the electrodes, a fact that provides the motivation for sampling electrical activation from as many sites as is technically possible. It must similarly be noted that some electrodes are almost inevitably faulty in experimentation and therefore generate what is referred to as bad leads. Bad leads are exemplified by excessive baseline drift, low signal-to-noise ratios (SNR), or even a lack of deflection for the whole cardiac electrical recording (Fig. 2.2). In this instance, bad leads must be either neglected during simulation or replaced by interpolated approximations.

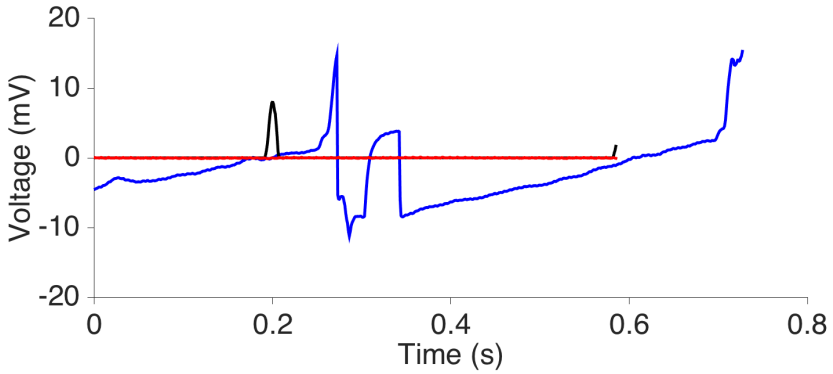

Figure 2.2: Bad leads present within canine cardiac recordings can be exemplified by baseline drift (blue), low SNR (black), or a lack of a signal (red).

CHAPTER 3

IMPLEMENTATION

This section outlines the general workflow required for registration of canine cardiac geometries to a human torso geometries followed by temporal dilation of the measured electrogram (EG) signals to reduce the resulting artifacts. A graphical representation of the pipeline is shown (Fig. 3.1).

3.1 Canine Cardiac Data Acquisition

Ten sets of canine cardiac epicardial potentials maps were attained from experiments using in situ, open-chest preparations with a sock of electrodes placed over the ventricles at a sampling rate of 1000 Hz. The sock electrode geometry contained 128, 247, or 490 electrodes, where the same sock geometry was used for multiple experiments to facilitate comparison of signals across experiments. Each canine cardiac data set contained one or more spontaneous beats triggered by the sinus node of the animal and at least one run of VF or VT, typically induced through specific, artificial stimulation protocols. All

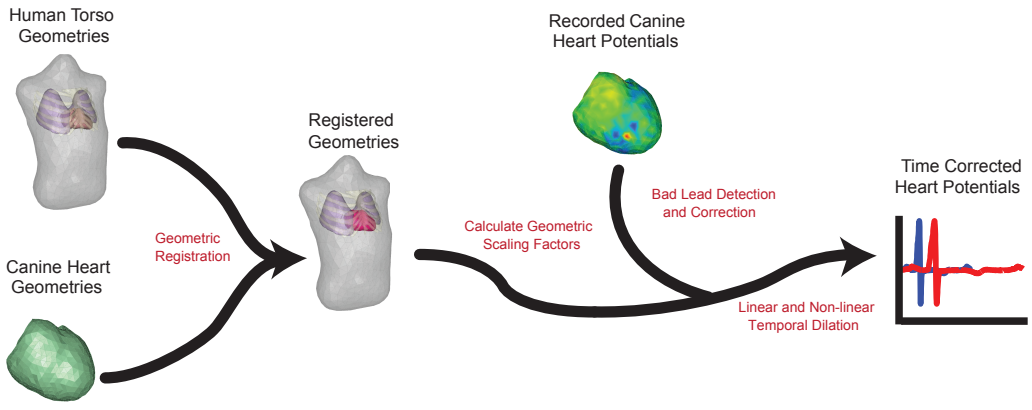

Figure 3.1: Pipeline for the temporal dilation of canine cardiac data.

recorded cardiac data were initially processed using baseline correction and band-pass filtering according to standard lab practices [22].

3.2 Geometrical Model Processing

Two geometric models of human torsos were created, in part through collaborations with other groups. The surfaces for Torso #1 were provided as part of the r We then used volume meshing tools in our own SCIRun software [23] and the open source Tetgen program [24] to create the associatewd tetrahedral mesh of this torso. Torso #2 was the product of simulation studies for implantable defibrillation, which we conducted together with scientists from Harvard University and the Childrens' Hospital Boston [25, 26]. To create the volume mesh for this torso, we used Cleaver2 meshing software [27]. Included in both torso geometries were the lungs, bone, blood volume, and pericardial heart tissue regions.

Canine cardiac sock geometries were modified to use with the human torso geometries. The cardiac socks used in the experiments were open near the base of the heart, so these sock geometries were capped with a partial ellipsoid with equivalent nodal spacing. By defining additional connectivity, the partial ellipsoid was integrated into the sock geometry. These capped sock geometries were then registered to each human torso heart geometry using a modified ICP algorithm with affine registration after an initial guess (Fig. 3.2) [28]. The initial guess was performed within SCIRun by visually aligning the two heart geometries using the left anterior descending artery as a guide to ensure proper convergence of the ICP algorithm. The modified ICP algorithm then registered using two point sets, one set describing the cardiac surface and a second set consisting of points along the major cardiac artery to resolve rotational ambiguities, with the same cost function applied to both. Each cardiac sock was registered to both human torso geometries for a total of 6 combinations. The cap was removed after registration, prior to further processing and temporal dilation.

3.3 Bad Lead Detection and Correction

We developed and applied a detection algorithm for bad leads in each set of canine cardiac data and corrected them prior to temporal dilation. The detection algorithm calculated metrics of maximum amplitude, an SNR on the entire signal, an SNR of a windowed baseline section of the PQ or RT segment, and a neighborhood correlation coefficient between each electrode and those at the immediately neighboring points, as defined by the triangular mesh [29]. We first carried out manual evaluation of comparison metrics and then identified cutoff values for each that robustly identified bad leads.

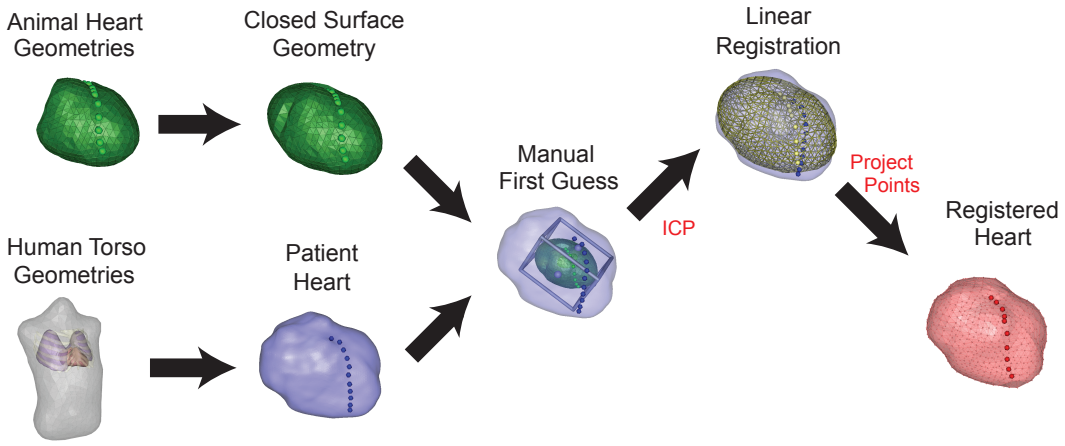

Figure 3.2: Pipeline for registering canine sock geometries to human torso geometries. The ICP algorithm first requires an initial guess to align corresponding points on the left anterior descending artery.

Once bad leads were detected, trilinear interpolation was used to replace the bad lead with a new signal based on the electrical potentials of neighboring recordings. Trilinear scattered interpolation was implemented over the heart surface (Fig. 3.3). First, a Delauney triangulation was created using both primary and secondary neighbors surrounding the bad lead [30]. Neighborhood connectivity is defined within the original sock electrode geometry. A triangle that encloses the original bad lead, defined using three neighboring points, is then selected from the triangulation. Each time step in the canine cardiac signal is then interpolated as a combination of the three neighbors weighted on spatial proximity.

3.4 Dilation of Cardiac Signals

Temporal dilation of the cardiac signals was based on the geometric registration of the canine hearts to the human hearts attained from Torso #1 and #2, where the scaling factors of dilation were based on the changes in edge lengths of the geometry. The global scaling factor was found as the median change in length over all edges of the whole sock (Eq. 3.1). The local scaling, by contrast, was determined by the mean change in edge length of the edges connected to each node (Eq. 3.2). All scaling factors were represented by a rational ratio, defined as the new edge length over the original, shorter edge length. Both sets of scaling factors were found for each of the 20 combinations and used to perform temporal dilation.

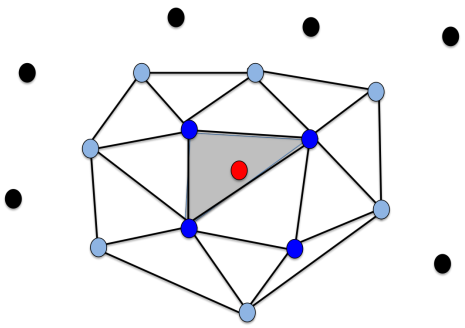

Figure 3.3: A schematic of trilinear scattered interpolation of bad leads (red) using triangulation projected in 2D. A Delauney triangulation based on a neighborhood region, using both primary (dark blue) and secondary (light blue) neighbors, is used to select a triangle (gray) surrounding the bad lead. Nodes of the selected triangle are used to generate a distance-weighted sum.

$$g = median\left(\frac{d(j)_o}{d(j)_{reg}}\Big|_{j=1}^{E}\right) \tag{3.1}$$

$$l(i) = median\left(\frac{d(k)_o}{d(k)_{reg}}\Big|_{k=1}^{P(i)}\right)\Big|_{i=1}^{N} \tag{3.2}$$

g: global scaling factor

l: local scaling factor for each node on sock electrode geometry

d_o: original edge length between nodes on sock electrode geometry

d_{reg}: edge length between nodes on sock electrode geometry after registration

E: total number of edges in sock electrode geometry

P: total number of primary neighbors for given node

N: total number of nodes in sock electrode geometry

For both linear and nonlinear dilation techniques, original and dilated activation and recovery times were required to ensure that the activation and recovery times were scaled appropriately as the original times multiplied by the local or global scaling factor. The activation and recovery times were calculated using a self-written automatic detection function on the QRS complex and T wave, respectively. The automatic detection was based on finding the minimum and maximum derivatives in the waveform of a polynomial curve fit for activation or recovery, respectively, and required input parameters of step-size

and confidence interval. To ensure proper detection, the parameters were optimized before and after dilation. The QRS complex and the T wave were windowed using manual selection on the squared sum over all leads on the cardiac surface.

After calculation of the scaling factors, temporal dilation was performed both linearly and nonlinearly (Fig. 3.4). Linear temporal dilation was performed by resampling the entire time signal for the cardiac surface by either the local or global scaling factors [31]. Linear temporal dilation was implemented for both sinus beats and arrhythmia recordings in each cardiac data set. Any discrepancies in the number of samples in the dilated signals across leads were made up by terminal padding of the signals with zeros.

Nonlinear temporal dilation was also implemented for the sinus beats in each canine cardiac data set using both local and global scaling factors. In this case, certain segments of the EGs were dilated individually to ensure that the QRS complex and T-wave durations remained the same length even after dilation (Fig. 3.4). To achieve this, only the components of the time signals outside the QRS complex and T wave underwent dilation and by different scaling factors. The entire segment before the QRS complex was resampled by a ratio, termed r_1. A second segment between the QRS complex and the T-wave in the sinus

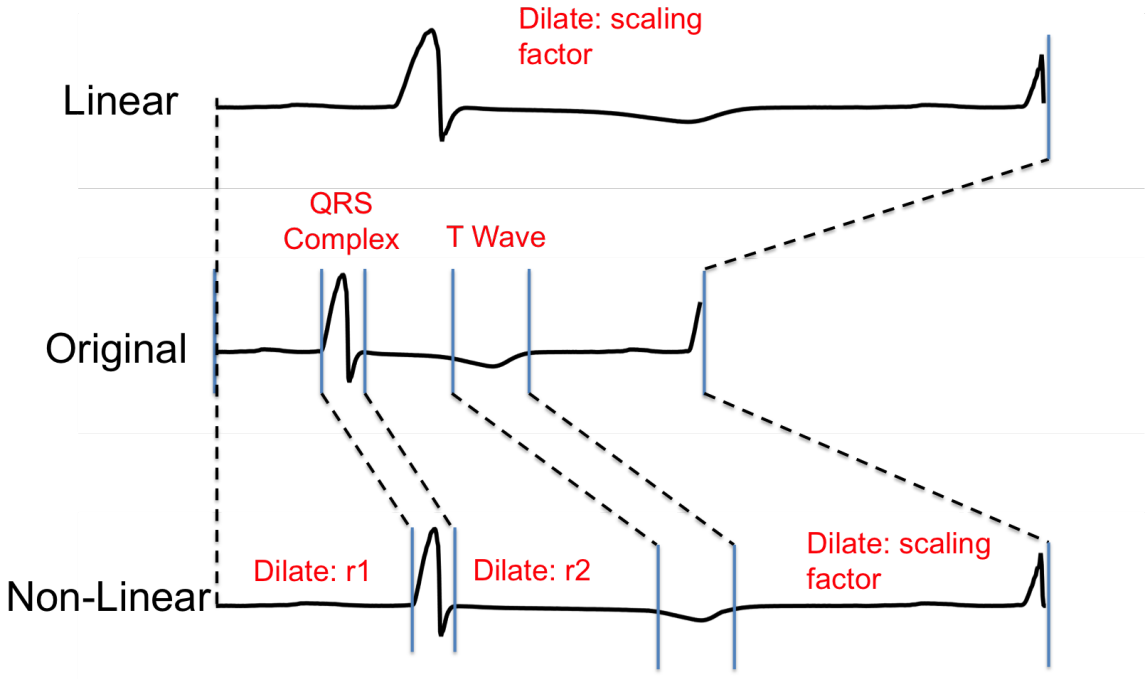

Figure 3.4: Schematic of nonlinear and linear temporal dilation. Linear dilation involves dilating the original signal (middle) by a signal scaling factor (top), while nonlinear temporal dilation (bottom) dilates segments outside the QRS complex and T-wave.

run was also resampled b using another ratio, termed r_2. These new ratios were a function of the original scaling factor, the start and end of the QRS complex and T wave, and the activation and recovery times (Eqs. 3.3 and 3.4). Everything after the end of T wave was dilated by either the original local or global scaling factor. These dilated segments were then concatenated with the QRS complex and the T-wave to reconstruct a signal that had an overall nonlinear dilation.

$$r_1 = \frac{AT_o(scalingfactor) - QRS_{start}}{AT_o - QRS_{start}} \tag{3.3}$$

$$r_2 = \frac{T_o(scalingfactor) - QT_{start} - AT_o(scalingfactor) - QRS_{end}}{T_o - QT_{start} - AT_o - QRS_{end}} \tag{3.4}$$

QRS_{start}: original start of the QRS complex
AT_o: original activation time
T_o: original recovery time
QT_{start}: start of the T-wave
QRS_{end}: original end of the QRS complex

Due to the resampling method used in nonlinear temporal dilation, artifacts appeared at both ends of each dilated segment. To account for such artifacts and maintain a fluent signal after concatenating the segments, the segments were resampled with an additional five data points on each end. After resampling, the padded segment was then cropped to maintain the original size. Similar to linear temporal dilation using local scaling factors, where it was necessary to preserve signal durations, the resultant signals were also padded with zeros.

3.5 Evaluation of the Dilated Cardiac Signals

Canine cardiac signals before dilation were evaluated for general morphology characteristics including total activation time (TAT) and activation recovery interval (ARI) for each sinus beat. TAT was found as the mean difference between the earliest and latest activation times in the ventricles, and ARI was found as the mean difference between activation and recovery times in the ventricles. Furthermore, the median CV for cardiac propagation was found in the ventricles, calculated as the median value of the change in activation

time divided by distance between two electrodes connecting every edge in the entire sock geometry. Dilated cardiac signals, registered for both geometries, were evaluated for the same characteristics and compared to the values found before dilation. Such metrics were further compared to known human and canine values. A qualitative comparison was also made using activation maps generated by showing the activation at every node on the electrode sock geometry. Activation timing was from the start of the QRS complex.

CHAPTER 4

RESULTS

This section outlines the results of temporal dilation on canine cardiac recordings using both local and global scaling factors. Temporal dilation techniques were evaluated using wave morphology, activation maps and quantitative metrics like CV, TAT, and ARI.

4.1 Scaling Factors

All scaling factors, both local and global, calculated during geometric transformations are listed in Table 4.1. The mean of local scaling factors were comparable to global scaling factors for all geometric combinations (Table 4.1).

For all three sock geometries, the highest deformation of local scaling for registration to Torso #1 occurs at the apex of the heart and along the basal aspects of the ventricles (Fig. 4.1). The range of local scaling factors increased with increasing number of electrodes in the sock geometry. Results are comparable for registration to Torso #2.

4.2 Qualitative Comparison of Temporal Dilation

Linear temporal dilation for both sinus and arrhythmic EGs maintained the general wave morphology (Fig. 4.2). Nonlinear temporal dilation, on the other hand, resulted in

Table 4.1: Global and mean local scaling factors for 128, 247, and 490 sock electrode geometries when registered to Torso #1 and Torso #2

Sock Geometry	Torso #1	Torso #2
	Global Scaling Factor	
128	1.48	1.64
247	1.64	1.84
490	1.57	1.71
	Local Scaling Factors	
128	1.49 ± 0.01	1.62 ± 0.01
247	1.66 ± 0.01	1.87 ± 0.01
490	1.58 ± 0.01	1.73 ± 0.01

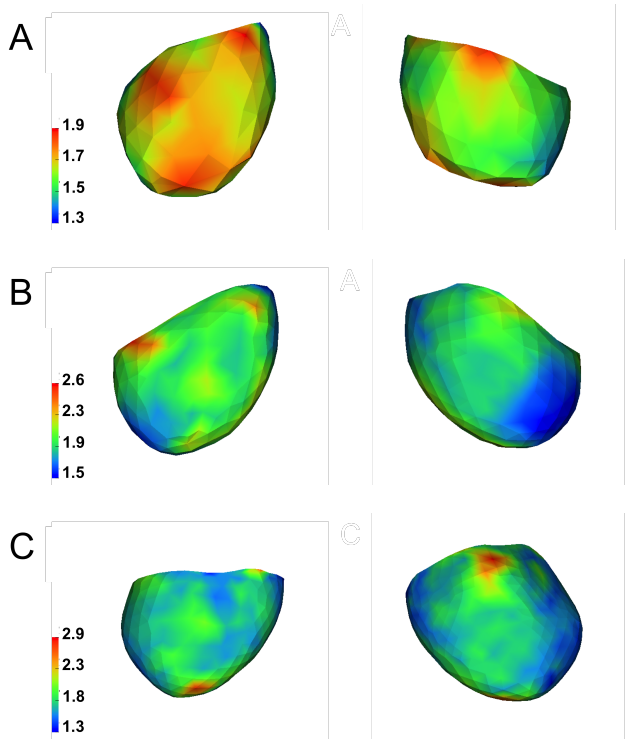

Figure 4.1: Local scaling factors mapped onto the 128 (A), 247 (B), and 490 (C) sock geometries registered to Torso #1. The scaling is the same for each respective subfigure.

the maintenance of the QRS complex and T-wave morphology with prolonged QT and ST segments (Fig. 4.2a).

Activation maps on the cardiac surface during sinus beat provided further means for qualitative comparison (Fig. 4.3). Both nonlinear and linear temporal dilation performed similarly, but nonlinear experienced earlier activation times due to the preservation of the QRS complex. When registered to either Torso #1 or Torso #2, global linear temporal dilation simply resulted in the same general activation pattern, but delayed (Figs. 4.3c and 4.3g). Local linear temporal dilation not only increased the general range of activation times, especially near the apex and basal aspects of the ventricles, but altered activation patterns (Figs. 4.3g and 4.3i).

4.3 Quantitative Evaluation of Cardiac Morphology

The mean CV, ARI, and TAT values across all 10 data sets for the original canine recordings were 33.41 ± 3.19 cm/s, 165.40 ± 12.64 ms, and 33.60 ± 3.94 ms, respectively. By comparison, the CV, ARI, and TAT mean values for all combinations of dilation or registration are shown in Table 4.2. Performing both nonlinear and linear temporal dilation

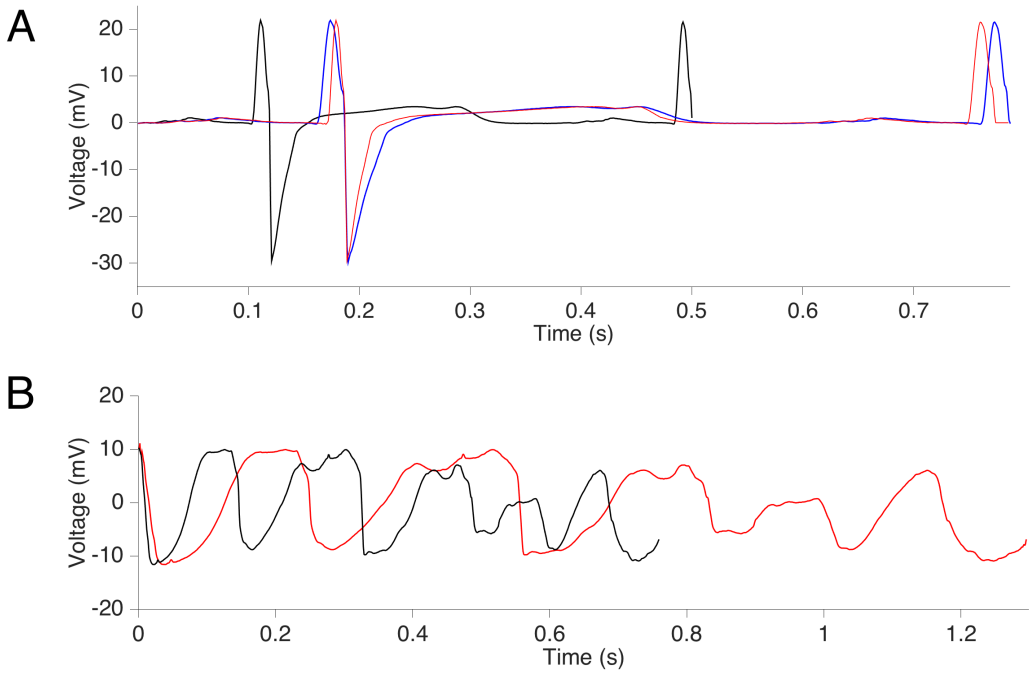

Figure 4.2: Temporal dilation using a global scaling factor of 1.71 on a sinus (A) and VF (B) recording from the 490 sock electrode geometry registered to Torso #1. The original (black) waveform is shown alongside the linearly (blue) and nonlinearly (red) dilated waveforms.

with a global scaling factor resulted in CV values that were only slightly elevated past the original mean. Both ARI and TAT, on the other hand, increased proportionally to the scaling factor. When performing temporal dilation with local scaling factors, however, CVs dropped and TAT increased drastically. The ARIs, in this case, remained relatively consistent using either local or global scaling factors. The metrics for linear and nonlinear dilation techniques were relatively similar.

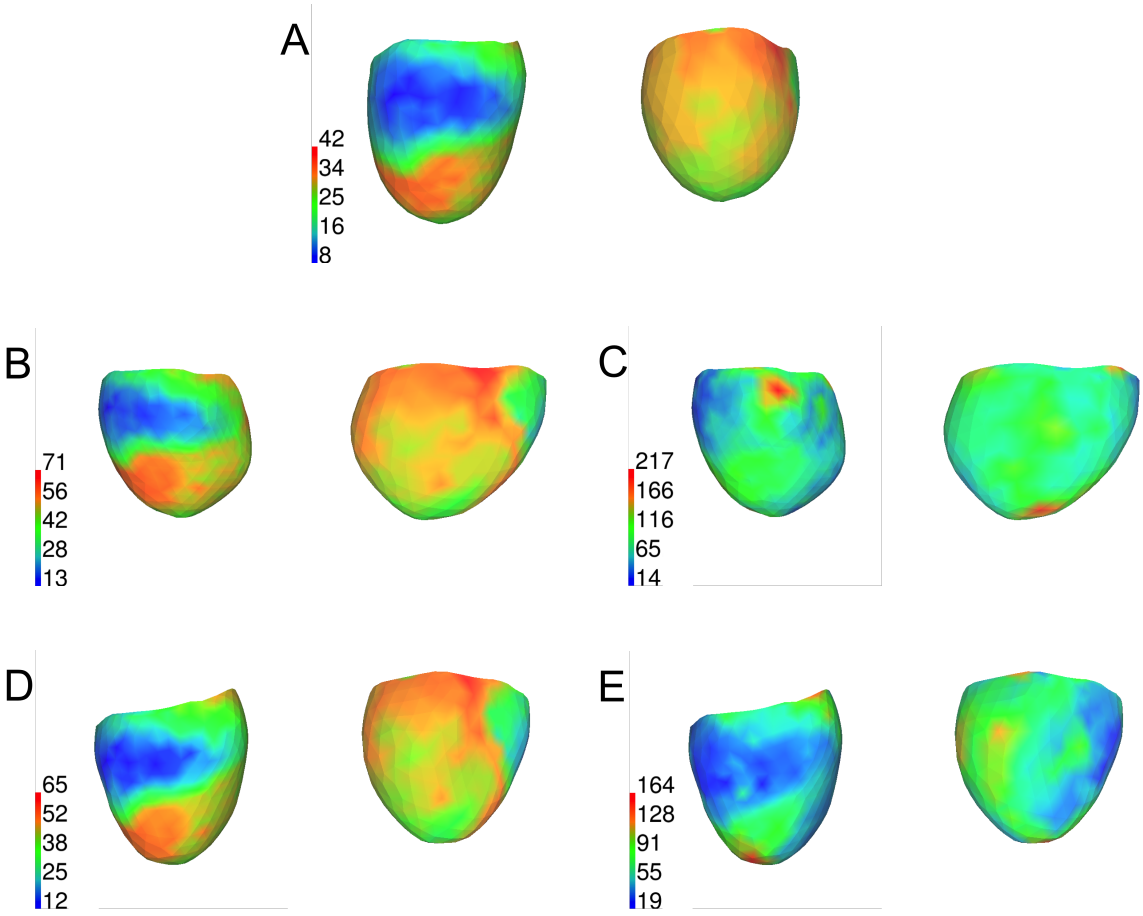

Figure 4.3: Activation maps for the original (A) and 490 sock electrode geometry registered to Torso #1 (B,C) or Torso #2 (D,E) after linear temporal dilation. Activation maps are shown using both global (B,D) and local (C,E) scaling factors. Scaling is shown in ms, where the scaling is the same for each respective subfigure.

Table 4.2: Mean CV, ARI, and TAT values across all 10 canine cardiac data sets for all combinations of registration, dilation, and scaling

Value	**Linear**		**Nonlinear**	
	Torso #1	Torso #2	Torso #1	Torso #2
		Global Scaling Factor		
CV (cm/s)	34.23 ± 3.34	34.67 ± 3.38	34.79 ± 3.58	35.24 ± 2.85
ARI (ms)	269.86 ± 25.58	250.82 ± 1.29	280.67 ± 23.62	252.67 ± 21.53
TAT (ms)	58.10 ± 6.59	53.50 ± 6.04	59.00 ± 6.52	52.30 ± 6.05
		Local Scaling Factors		
CV (cm/s)	17.34 ± 3.12	18.93 ± 2.95	17.33 ± 3.14	18.61 ± 2.64
ARI (ms)	271.06 ± 23.53	237.19 ± 23.33	283.09 ± 23.77	251.13 ± 19.80
TAT (ms)	265.70 ± 41.84	192.10 ± 24.08	268.70 ± 42.12	193.40 ± 24.36

CHAPTER 5

DISCUSSION

This study aimed to evaluate the technical feasibility of mapping cardiac electrophysiology signals from animal to human geometries and specifically to develop methods of temporal signal dilation to make them physiologically closer to human signals. The motivation for this approach was to generate electrophysiological data for human studies from animal data sets available in experiments. Temporal dilation was necessary to compensate for the spatial dilation that occurs when mapping from small animal hearts to relatively larger human hearts. We carried out this manipulation using both local and global scaling factors derived from the geometric mapping transformations. We compared the dilated cardiac signals using qualitative and quantitative metrics and summarize this comparison in this section. Other limitations of the methodology and future work are then addressed.

5.1 Physiological Comparisons Across Species

CV in dogs ranges from 21 cm/s to 53 cm/s depending on the orientation of the spread of activation, where 53 cm/s indicates CV along fibers [32]. The reported mean value in our studies of 33.41 cm/s falls functionally within this range. After temporal dilation using a global scaling factor, the CV approached the lower end of human conduction velocities in ventricular tissue, which range from 30 to 100 cm/s, also depending on fiber orientation and propagation direction [1]. Local scaling factors resulted in significantly lower CVs that were well outside the normal physiological range for humans.

The reported mean value for TAT of 33.6 ms that we found from our canine experiments was slightly above the normal range of 20 to 30 ms for dogs [33]. After applying temporal dilation with global scaling, the values for TAT when the same signals were mapped to human hearts were only slightly above the human physiological range of 30 to 50 ms (Table 4.2) [34]. When using local scaling, however, the values of TAT became unrealistically elevated (Table 4.2). The mean ARI time of 165.40 ms, from the canine cardiac recordings, was low for control canine cardiac recordings, but still remained physiologically relevant [35]. Throughout every form of temporal dilation we applied, ARI remained within the normal human range [36].

After temporal dilation, the general activation patterns on the epicardial surfaces were similar to those reported in the very few human studies with the earliest activation occurring on the epicardium between the apex and base and spreading outwards (Fig. 4.3) [37].

5.2 Evaluation of Temporal Dilation

The primary consideration for temporal dilation is the resulting usability of dilated signals in further cardiac applications. In general, linear temporal dilation, i.e., dilation that was applied consistently across the entire time course of the signal, could be used on both sinus and arrhythmic signals, critical for application in arrhythmia diagnostic and monitoring technology (Fig. 4.2). By contrast, the nonlinear temporal dilation we developed requires delineation of the signal into its separate components and applying different scaling to each component. The motivation for this approach was to preserve the time course of events that are likely preserved across size and species, the QRS complex and T wave (Fig. 4.2). However, as arrhythmic signals do not have preserved QRS complexes or, in extreme VF, it is impossible to even identify discrete waveforms; only a homogenous temporal dilation is feasible.

A further technical point of exploration was to compare results from a global scaling factor to a set of local factors derived at each node in the sock geometry. We expected global temporal dilation to perform worse than local due to the local spatial dilation that occurred during registration of the canine hearts to the human torso geometries. The ICP algorithm, used for such registration, causes a nonhomogenous change in edge length due to a nonlinear projection of points. The somewhat surprising finding was that local scaling factors resulted in drastically different CVs, TATs, and activation maps from those measured from the original canine cardiac data sets (Table 4.2, Fig. 4.3), and global scaling factors resulted in more physiologically relevant signals and quantitative parameters (Section 5.1).

There are multiple possible explanations for this discrepancy in the apparent accuracy of local versus global dilation. First, the local approach we employed was simple and did not take into account features such as local fiber orientation, propagation direction, or changes in the tissue near the nodal locations. Second, the values of key parameters of the spread of excitation we observed in experiments (CV, TAT, ARI) lay outside the normal range for canines so that we cannot be surprised that transformation of these signals to the human domain led to similarly unphysiologic values. Here, we did not carry out fresh experiments, nor could we reconstruct all the conditions that arose during past experiments, each of which included various forms of intervention meant to mimic pathophysiology. Lastly, though the

mapping of local scaling factors provides some indication (Fig. 4.1), we did not attempt to directly analyze the nature or extent of changes in edge lengths resulting from the geometric registration of canine hearts to human torso geometries. We did observe that some local scaling factors were quite dramatically different from the mean (Table 4.1, Fig. 4.1), and that the range of local scaling factors increased with a growing number of electrodes on the sock geometry (Fig. 4.1). Such variation in local scaling factors directly influenced the range and relative timing of activation times, as visually noticeable in activation maps (Fig. 4.3), and recovery times. Such an increase in range could explain the prolonged TAT durations, while the drastically different values of CV could be attributed to the relative change in timing of activation from one node to another.

5.3 Other Limitations in Methodology

The methodology has various limitations in addition to setting the parameters for temporal dilation. For example, in segmentation, the imaging modality can introduce noise because of poor image resolution and low soft tissue contrast [38]. Additionally, due to the variation and complexity of cardiac anatomy and pathology, cardiac segmentation can be both subjective and difficult [39]. Inaccuracies in the model representation of the actual geometries for both the torso and canine heart can lead to further downstream problems with registration, calculation of the scaling factors, and possible further cardiac applications. Registration is a source of additional error; for example, the ICP algorithm is guaranteed to converge to a local minima using optimization, but it does not necessarily mean that the registration will converge to the best possible alignment [19].

Another limitation of the methodology is errors in the detection and correction of bad leads due to setting of thresholds and choice of interpolation method. Since the bad lead algorithms are dependent on the somewhat arbitrarily established thresholds, the leads may be falsely classified. Manual classifications could result in greater accuracy, but they are not efficient for a large number of data sets. Also, trilinear interpolation used for bad lead correction resulted in slightly lower peaks than at surrounding neighbors due to averaging, although wave morphology was maintained.

The use of any overall metric of a complex process like cardiac activation is burdened by error and uncertainty from many sources. All depend on the automatic calculation of activation and recovery times, which can be influenced by the choice of function representing the actual wave shape as well as the associated parameters. In the specific setting of the dilated signals, we had to alter the choice of parameters due to reduced time derivatives.

Additionally, the CV was reported in only a single metric instead of along the different fiber orientations.

5.4 Future Work

Future work could aim to address some of the limitations of resampling and wave morphology detection as described for temporal dilation. First, different filters in the resampling technique could be implemented to possibly prevent the need for cropping during nonlinear dilation and therefore provide a smoother signal. Different types of low pass filters have already been explored, but more complex filters allowing subband decomposition could help maintain signal integrity [31]. The manual selection of the QRS complex and T wave could be avoided in nonlinear temporal dilation by using QRS and T wave detection algorithms [40].

Other aspects of the methodology could also be refined such as bad lead detection and activation and recovery time estimation. Bad lead detection could be improved by adding additional metrics that detect different types of bad leads. Additionally, thresholds could be further tuned to ensure that the probability of false classification in bad lead detection is lowered. Similarly, function parameters used for detection of activation and deactivation times detection could be further refined to ensure limited variability in calculation.

Further validation is required to ensure that the temporally dilated canine cardiac signals resemble human recordings in terms of arrhythmias. Validation could be performed through the use of cardiac simulation software such as CARP [41]. Using such tools, a simulation that induces an arrhythmia could first be conducted on both the original and registered canine sock geometries. The cardiac potentials attained from the simulation on the original geometry would then be dilated and compared to the output from the simulation on the registered geometries. Such comparison would not only allow customization of the specific ventricular arrhythmia to be compared, but could also highlight further differences between human and dilated canine recordings.

5.5 Conclusion

We have developed a pipeline that performs geometric registration and fitting between canine and human hearts and then applies subsequent temporal dilation on both sinus and arrhythmic canine cardiac signals (Fig. 3.1). With certain limitations, globally homogeneous temporal dilation allowed for the manipulation of canine cardiac signals to physiologically relevant ranges in humans in terms of CV, ARI, and TAT (Section 5.1).

Local temporal dilation did not generate physiologically relevant cardiac signals (Section 5.1).

Temporal dilation using global scaling factors should be an important consideration whenever mapping cardiac potentials to a differently sized geometry because it allows for the preservation of physiological parameters of conduction that are spatially dependent, such as CV (Section 5.1). Since geometric registration of canine geometries to humans can be used to generate much larger and more varied databases of ventricular arrhythmias than will ever be possible from human experiments, temporal dilation can be applicable to a variety of cardiac applications. The primary cardiac simulations that could benefit from the proposed pipeline of temporal dilation include the ECG forward and inverse problems and placement and testing of ICDs (Section 2.1) [42, 43]. Thus, temporal dilation can be used to generate a larger database to train and validate new diagnostic and monitoring tools in electrocardiology.

REFERENCES

[1] A. M. Katz, *Physiology of the Heart*. Lippincott Williams & Wilkins, 2010.

[2] J. Malmivuo and R. Plonsey, *Bioelectromagnetism: Principles and Applications of Bioelectric and Biomagnetic Fields*. Oxford University Press, USA, 1995.

[3] P. Taggart, P. M. Sutton, M. R. Boyett, H. Swanton *et al.*, "Human ventricular action potential duration during short and long cycles rapid modulation by ischemia," *Circulation*, vol. 94, no. 10, pp. 2526–2534, 1996.

[4] R. Coronel, J. Fiolet, F. Wilms-Schopman, A. Schaapherder, T. Johnson, L. Gettes, and M. Janse, "Distribution of extracellular potassium and its relation to electrophysiologic changes during acute myocardial ischemia in the isolated perfused porcine heart." *Circulation*, vol. 77, no. 5, pp. 1125–1138, 1988.

[5] R. M. Shaw and Y. Rudy, "Electrophysiologic effects of acute myocardial ischemia a mechanistic investigation of action potential conduction and conduction failure," *Circulation Research*, vol. 80, no. 1, pp. 124–138, 1997.

[6] J. De Bakker, F. Van Capelle, M. J. Janse, S. Tasseron, J. T. Vermeulen, N. De Jonge, and J. R. Lahpor, "Slow conduction in the infarcted human heart.'zigzag'course of activation." *Circulation*, vol. 88, no. 3, pp. 915–926, 1993.

[7] M. AlGhatrif and J. Lindsay, "A brief review: history to understand fundamentals of electrocardiography," *Journal of Community Hospital Internal Medicine Perspectives*, vol. 2, no. 1, 2012.

[8] R. M. John, U. B. Tedrow, B. A. Koplan, C. M. Albert, L. M. Epstein, M. O. Sweeney, A. L. Miller, G. F. Michaud, and W. G. Stevenson, "Ventricular arrhythmias and sudden cardiac death," *The Lancet*, vol. 380, no. 9852, pp. 1520–1529, 2012.

[9] R. MacLeod and M. Buist, "The forward problem of electrocardiography," in *Comprehensive Electrocardiology*, P. Macfarlane, A. van Oosterom, O. Pahlm, P. Kligfield, M. Janse, and J. Camm, Eds. Springer Verlag, 2010.

[10] A. J. Pullan, L. K. Cheng, M. P. Nash, A. Ghodrati, R. MacLeod, and D. H. Brooks, "The inverse problem of electrocardiography," in *Comprehensive Electrocardiology*. Springer, 2010, pp. 299–344.

[11] W. Trautwein, D. G. Kassebaum, R. M. Nelson, and H. H. Hecht, "Electrophysiological study of human heart muscle," *Circulation Research*, vol. 10, no. 3, pp. 306–312, 1962.

[12] R. S. Macleod, J. Stinstra, S. Lew, R. T. Whitaker, D. Swenson, M. Cole, J. Krüger, D. Brooks, and C. R. Johnson, "Subject-specific, multiscale simulation of electrophysiology: a software pipeline for image-based models and application examples," *Philosophical Transactions of the Royal Society of London A: Mathematical, Physical*

and Engineering Sciences, vol. 367, no. 1896, pp. 2293–2310, 2009.

[13] N. R. Pal and S. K. Pal, "A review on image segmentation techniques," *Pattern Recognition*, vol. 26, no. 9, pp. 1277–1294, 1993.

[14] Y. Zhang and C. Bajaj, "Finite element meshing for cardiac analysis," ICES Technical Report 04-26, University of Texas, Austin, Tech. Rep., 2004.

[15] M. Bern and D. Eppstein, "Mesh generation and optimal triangulation," in *Computing in Euclidean Geomtry*, F. Hwang and D. Du, Eds. World Scientific, 1992.

[16] T. Baker, "Delaunay-voronoi methods," in *Handbook of Grid Generation*, J. Thompson, B. Soni, and N. Weatherill, Eds. Boca Raton: CRC Press, 1999, p. 16.116.11.

[17] J. Challis, "A procedure for determining rigid body transformation parameters," *Journal of Biomechanics*, vol. 28, no. 6, pp. 733–737, 1995.

[18] J. A. Maintz and M. A. Viergever, "A survey of medical image registration," *Medical Image Analysis*, vol. 2, no. 1, pp. 1–36, 1998.

[19] P. J. Besl and N. D. McKay, "Method for registration of 3-d shapes," in *Robotics-DL tentative*. International Society for Optics and Photonics, 1992, pp. 586–606.

[20] J. W. Hurst, "Naming of the waves in the ecg, with a brief account of their genesis," *Circulation*, vol. 98, no. 18, pp. 1937–1942, 1998.

[21] L. Biel, O. Pettersson, L. Philipson, and P. Wide, "Ecg analysis: a new approach in human identification," *Instrumentation and Measurement, IEEE Transactions on*, vol. 50, no. 3, pp. 808–812, 2001.

[22] S. Shome, J. Stinstra, C. Henriquez, and R. MacLeod, "Influence of extracellular potassium and reduced extracellular space on conduction velocity during acute ischemia: a simulation study," *Journal of Electrocardiology*, vol. 39, no. 4, pp. S84–S85, 2006.

[23] R. MacLeod, D. Weinstein, J. D. de St. Germain, D. Brooks, C. Johnson, and S. Parker, "SCIRun/BioPSE: Integrated problem solving environment for bioelectric field problems and visualization," in *IEEE International Symposium on Biomedical Imaging (ISBI)*, IEEE. IEEE Press, 2004.

[24] H. Si and K. Gaertner, "Meshing piecewise linear complexes by constrained delaunay tetrahedralizations," in *Proceedings of the 14th International Meshing Roundtable*, 2005, pp. 147–163.

[25] M. Jolley, J. Stinstra, S. Pieper, R. MacLeod, D. H. Brooks, F. Cecchin, and J. K. Triedman, "A computer modeling tool for comparing novel icd electrode orientations in children and adults," *Heart Rhythm*, vol. 5, no. 4, pp. 565–572, 2008.

[26] M. Jolley, J. Stinstra, J. Tate, S. Pieper, R. MacLeod, L. Chu, P. Wang, and J. K. Triedman, "Finite element modeling of subcutaneous implantable defibrillator electrodes in an adult torso," *Heart Rhythm*, vol. 7, no. 5, pp. 692–698, 2010.

[27] CIBC, 2015, cleaver: A MultiMaterial Tetrahedral Meshing Library and Application. Scientific Computing and Imaging Institute (SCI), Download from:

http://www.sci.utah.edu/cibc/software.html.

[28] D. Chetverikov, D. Svirko, D. Stepanov, and P. Krsek, "The trimmed iterative closest point algorithm," in *Pattern Recognition, 2002. Proceedings. 16th International Conference on*, vol. 3. IEEE, 2002, pp. 545–548.

[29] R. A. Fisher, *Statistical Methods for Research Workers*. Genesis Publishing Pvt Ltd, 1925.

[30] H. Edelsbrunner, *Geometry and Topology for Mesh Generation*. Cambridge University Press, 2001.

[31] L. R. Rabiner, *Multirate Digital Signal Processing*. Prentice Hall PTR, 1996.

[32] D. E. Roberts, L. T. Hersh, and A. M. Scher, "Influence of cardiac fiber orientation on wavefront voltage, conduction velocity, and tissue resistivity in the dog." *Circulation Research*, vol. 44, no. 5, pp. 701–712, 1979.

[33] J. D. Hill and E. N. Moore, "Epicardial excitation studies in dogs with congenital right ventricular hypertrophy," *Circulation Research*, vol. 20, no. 6, pp. 649–657, 1967.

[34] D. M. Cassidy, J. A. Vassallo, F. E. Marchlinski, A. E. Buxton, W. J. Untereker, and M. E. Josephson, "Endocardial mapping in humans in sinus rhythm with normal left ventricles: activation patterns and characteristics of electrograms." *Circulation*, vol. 70, no. 1, pp. 37–42, 1984.

[35] C. W. Haws and R. L. Lux, "Correlation between in vivo transmembrane action potential durations and activation-recovery intervals from electrograms. effects of interventions that alter repolarization time." *Circulation*, vol. 81, no. 1, pp. 281–288, 1990.

[36] A. M. Yue, J. R. Paisey, S. Robinson, T. R. Betts, P. R. Roberts, and J. M. Morgan, "Determination of human ventricular repolarization by noncontact mapping validation with monophasic action potential recordings," *Circulation*, vol. 110, no. 11, pp. 1343–1350, 2004.

[37] D. Durrer, R. T. Van Dam, G. Freud, M. Janse, F. Meijler, and R. Arzbaecher, "Total excitation of the isolated human heart," *Circulation*, vol. 41, no. 6, pp. 899–912, 1970.

[38] A. J. Prassl, F. Kickinger, H. Ahammer, V. Grau, J. E. Schneider, E. Hofer, E. J. Vigmond, N. A. Trayanova, G. Plank *et al.*, "Automatically generated, anatomically accurate meshes for cardiac electrophysiology problems," *IEEE Transactions on Biomedical Engineering*, vol. 56, no. 5, pp. 1318–1330, 2009.

[39] D. Kang, J. Woo, P. J. Slomka, D. Dey, G. Germano, and C.-C. J. Kuo, "Heart chambers and whole heart segmentation techniques: review," *Journal of Electronic Imaging*, vol. 21, no. 1, pp. 010 901–1, 2012.

[40] J. Pan and W. J. Tompkins, "A real-time qrs detection algorithm," *IEEE Transactions on Biomedical Engineering*, no. 3, pp. 230–236, 1985.

[41] E. J. Vigmond, M. Hughes, G. Plank, and L. J. Leon, "Computational tools for modeling electrical activity in cardiac tissue," *Journal of Electrocardiology*, vol. 36,

pp. 69–74, 2003.

[42] R. M. Gulrajani, "The forward and inverse problems of Electrocardiography," *IEEE Engineering in Medicine and Biology Magazine*, vol. 17, no. 5, pp. 84–101, 1998.

[43] M. Jolley, J. Stinstra, S. Pieper, R. MacLeod, D. H. Brooks, F. Cecchin, and J. K. Triedman, "A computer modeling tool for comparing novel ICD electrode orientations in children and adults," *Heart Rhythm*, vol. 5, no. 4, pp. 565–572, 2008.

[44] P. M. Van Dam, T. F. Oostendorp, and A. Van Oosterom, "Ecgsim: interactive simulation of the ecg for teaching and research purposes," in *2010 Computing in Cardiology*. IEEE, 2010, pp. 841–844.

[45] A. Van Oosterom, "Genesis of the t wave as based on an equivalent surface source model," *Journal of Electrocardiology*, vol. 34, no. 4, pp. 217–227, 2001.